



Robust high-dynamic-range vector magnetometry with nitrogen-vacancy centers in diamond F

Cite as: Appl. Phys. Lett. **112**, 252406 (2018); <https://doi.org/10.1063/1.5034216>

Submitted: 10 April 2018 . Accepted: 21 May 2018 . Published Online: 22 June 2018

Hannah Clevenson , Linh M. Pham, Carson Teale, Kerry Johnson, Dirk Englund , and Danielle Braje

COLLECTIONS

F This paper was selected as Featured



View Online



Export Citation



CrossMark

ARTICLES YOU MAY BE INTERESTED IN

[Tutorial: Magnetic resonance with nitrogen-vacancy centers in diamond—microwave engineering, materials science, and magnetometry](#)

Journal of Applied Physics **123**, 161101 (2018); <https://doi.org/10.1063/1.5011231>

[Microwave-free magnetometry with nitrogen-vacancy centers in diamond](#)

Applied Physics Letters **109**, 053505 (2016); <https://doi.org/10.1063/1.4960171>

[Electric control of cooperative polariton dynamics in a cavity-magnon system](#)

Applied Physics Letters **112**, 262401 (2018); <https://doi.org/10.1063/1.5024336>



Measure Ready
M91 FastHall™ Controller

A revolutionary new instrument
for complete Hall analysis

 Lake Shore
CRYOTRONICS

Robust high-dynamic-range vector magnetometry with nitrogen-vacancy centers in diamond

Hannah Clevenson,^{1,2,a)} Linh M. Pham,^{2,a)} Carson Teale,^{1,2,a)} Kerry Johnson,² Dirk Englund,¹ and Danielle Braje²

¹Massachusetts Institute of Technology, Cambridge, Massachusetts 02139, USA

²MIT Lincoln Laboratory, Lexington, Massachusetts 02420, USA

(Received 10 April 2018; accepted 21 May 2018; published online 22 June 2018)

We demonstrate a robust, scale-factor-free vector magnetometer, which uses a closed-loop frequency-locking scheme to simultaneously track Zeeman-split resonance pairs of nitrogen-vacancy (NV) centers in diamond. This technique offers a three-orders-of-magnitude increase in dynamic range compared to open-loop methodologies; is robust against fluctuations in temperature, resonance linewidth, and contrast; and allows for simultaneous interrogation of multiple transition frequencies. By directly detecting the resonance frequencies of NV centers oriented along each of the diamond's four tetrahedral crystallographic axes, we perform full vector reconstruction of an applied magnetic field. *Published by AIP Publishing.* <https://doi.org/10.1063/1.5034216>

Quantum magnetometers have seen rapid advancement in the past two decades, with total-field sensitivities now rivaling those of cryogenic SQUIDS.¹ The nitrogen-vacancy (NV) color center in diamond is a particularly promising platform for a new class of quantum magnetic sensor that combines the long-term stability of an atom-like system with inherent vector capability in a compact, solid-state package. Similar to atomic magnetometers,² the NV center ties external field measurements to fundamental constants through Zeeman splitting of quantized energy levels.³ The solid-state platform facilitates the incorporation of a high density of NV centers [up to 10^{18} cm^{-3} (Refs. 4–6)] into a compact sensor volume. Furthermore, the tetrahedral structure of the diamond crystal lattice allows such devices to directly sense the magnetic field vector,^{7–9} an advantage over the inherently scalar measurements of traditional atomic magnetometers. The combination of these characteristics in a single magnetic sensor is transformational for a wide variety of magnetometry applications, ranging from all-magnetic navigation^{10,11} to geological surveys¹² to magnetic mapping of archaeological sites¹³ to locating unexploded ordnance.^{14,15}

In this work, we employ a frequency-locking magnetic sensing scheme to directly measure NV resonance frequencies.^{16,17} Using custom-built electronics to address a pair Zeeman-split resonance simultaneously, we decouple magnetic field measurements from temperature, important for field applications where careful temperature control is not plausible. We show the immunity of this scale-factor-free measurement technique to variable parameters such as microwave (MW) and laser intensity noise and perform real-time magnetic sensing with a high dynamic range. This capability is particularly necessary for non-stationary vector magnetic sensors, where rotation in an ambient field (e.g., Earth's field) may sweep field projections over $>100 \mu\text{T}$. Finally, we apply the frequency-locking technique to an NV ensemble and perform measurements along all four crystallographic axes in rapid sequence to reconstruct the full magnetic field vector.

This demonstration of robustness against non-magnetic noise, high dynamic range, and vector capability in a single magnetic sensing device marks a significant advance in transitioning lab-based systems to practical sensors operating in situations with limited control over environmental factors such as vibration, temperature, and ambient magnetic field.

The operating principle of the NV-based magnetometer³ relies on the spin-triplet ground state of the NV fine structure [Fig. 1(a)]. Under no external magnetic field, spin-spin interactions shift the $m_s = \pm 1$ sublevels from the $m_s = 0$ sublevel by the zero field splitting $\Delta \approx 2.87 \text{ GHz}$ at room temperature.¹⁸ In the presence of an external magnetic field, the $m_s = \pm 1$ sublevels are shifted by the Zeeman effect. In the limit where the component of the magnetic field transverse to the NV symmetry axis is negligible, the frequencies of $m_s = 0 \rightarrow \pm 1$ transitions are given by¹⁹

$$f_{0\pm} \approx \Delta + \beta_T \delta_T \pm \gamma B_{\text{NV}}, \quad (1)$$

where $\beta_T \approx -74 \text{ kHz/K}$ near room temperature,²⁰ δ_T is the temperature offset from 300 K during the measurement, $\gamma = g_e \mu_B / h \approx 28 \text{ Hz/nT}$ is the NV gyromagnetic ratio,¹⁹ and B_{NV} is the projection of the applied magnetic field along the NV symmetry axis.

A common method for sensing magnetic fields with NV centers relies on monitoring the optically detected magnetic resonance (ODMR) spectrum, measured by applying continuous above-band optical excitation and simultaneously sweeping the frequency of an applied microwave (MW) field. The optical excitation polarizes the NV center into the more fluorescent $m_s = 0$ spin state, and when the MW field is on resonance with an $m_s = 0 \rightarrow \pm 1$ transition, there is a decrease in the fluorescence intensity that manifests as a dip in the ODMR spectrum [Fig. 1(b)]. By simultaneously measuring both $m_s = 0 \rightarrow \pm 1$ transition frequencies, the effects of temperature and magnetic field can be decoupled to first order, as seen in Eq. (1). This approach can be extended to achieve vector magnetometry by measuring the ODMR spectrum of an NV ensemble to determine the resonance frequencies of all four NV axes. In this case, it is necessary to

^{a)}H. Clevenson, L. M. Pham, and C. Teale contributed equally to this work.

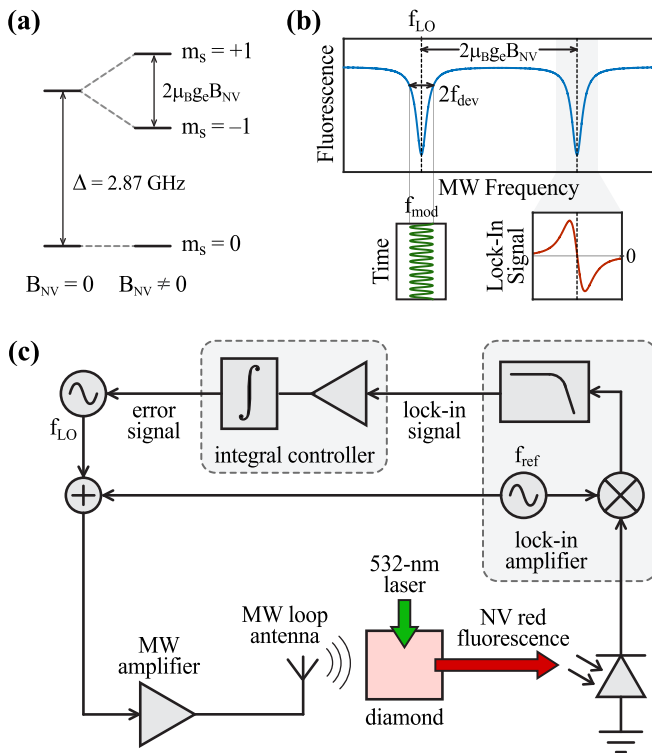


FIG. 1. Simplified electronic state energy level diagram (a) and optically detected magnetic resonance spectrum (b) of an NV electronic spin in the presence of an applied magnetic field B_{NV} . The microwave signal f_{mod} is generated by modulating f_{LO} at frequency f_{ref} with depth f_{dev} . The demodulated lock-in signal is shown for f_{LO} near an NV resonance, illustrating that the lock-in signal is zero when f_{LO} is directly on resonance. (c) Signal path for a single frequency locked loop.

consider additional shifts in the NV resonances due to non-negligible transverse magnetic field components in order to properly reconstruct the full vector magnetic field.

Previous demonstrations of ODMR-based NV magnetometry measured full spectra and performed fits to extract the NV resonance frequencies.^{7,8} While this method is able to access the full dynamic range of the NV center [>1 T (Ref. 21)] it also involves spending a large fraction of the measurement time monitoring non-information-containing, off-resonance signal and is subsequently prohibitively slow for some applications. Fitting the curves also introduces latency that may be incompatible with real-time sensing. More recent demonstrations used lock-in techniques to continuously monitor a single resonance on the approximately linear derivative section of the spectral feature, from which small resonance frequency shifts were detected by applying pre-calibrated scale factors.^{6,22–24} However, this second approach is limited to the approximately linear regime of the lock-in signal, resulting in a dynamic range of a few μ T. Furthermore, this method is inherently dependent on phenomenological variables; in particular, the scale factor is influenced by the NV resonance linewidth and contrast, both of which are affected by optical pump power, MW power, and detection efficiency.²⁵ These variables are different for each device and will drift over time, consequently requiring periodic recalibration.

Here, we present a closed-loop system that directly locks the MW drive field to one or more NV resonances, thus isolating the magnetic field measurement from the phenomenological variables that determine the scale factor of

previous lock-in-based approaches. Furthermore, by virtue of locking to the NV resonance frequency, the measurement is always performed in the approximately linear regime of the lock-in signal, enabling maximal sensitivity over the full dynamic range of the NV center. This frequency-locking technique is similar to that demonstrated recently on single NV centers in diamond,^{16,17} where sequential measurements of both resonance frequencies can be achieved via MW switching.¹⁶ However, while performing measurements sequentially provides some tolerance against temperature-coupled noise, this differential detection scheme is only effective at rejecting thermal fluctuations that much slower than the MW switching speed. We extend the frequency-locking technique to perform measurements on multiple NV resonances simultaneously, as is necessary for decoupling temperature from magnetic field over the full measurement bandwidth, and apply it to an NV ensemble to extract the magnetic field vector, thus demonstrating a capability not inherent to single NV centers.

Figure 1(c) shows a diagram of the signal path of a frequency locked loop for a single NV resonance. Note that while the single-channel case is discussed here for simplicity, simultaneous monitoring of $n > 1$ NV resonances is achieved straightforwardly by incorporating additional frequency channels. A signal generator outputs a MW signal frequency, f_{LO} , which is tuned to minimize the error on the feedback compensator. The MW signal is modulated at frequency f_{ref} with depth f_{dev} to produce a time-dependent frequency $f_{mod}(t)$ given by

$$f_{mod}(t) = f_{LO} + f_{dev} \cos(2\pi f_{ref} t). \quad (2)$$

The signal is sent to an antenna which drives the NV spin ensemble with the modulated MW field. The fluorescence signal from the diamond sample is detected with a photodetector and demodulated by a lock-in amplifier. We set the phase of the lock-in amplifier such that the in-phase component of the lock-in signal is positive (negative) if f_{LO} is slightly below (above) the NV transition frequency, whereas the lock-in signal is zero when f_{LO} is directly on resonance with the NV transition frequency [see Fig. 1(b)]. A feedback compensator, consisting of a discrete integral controller, produces an error signal from the lock-in signal. The error signal in turn provides feedback to adjust the MW source frequency f_{LO} and lock it to the center of the NV resonance. This closed loop system accurately tracks the resonant frequency in steady-state, and only the dynamics of the transient response are influenced by non-fundamental experimental parameters (see [supplementary material](#) for detailed derivation). Assuming appropriate tuning of the feedback gain parameter, the measurement bandwidth of this frequency-locking technique is set by the lock-in time constant, which is in turn bound by the modulation frequency. Due to limitations in the NV response bandwidth, measurement sensitivity degrades for modulation frequencies >20 kHz,^{6,22} resulting in a trade-off between measurement speed and sensitivity. To extend this technique to an n -frequency-channel implementation, each NV resonance is modulated at a different frequency $f_{ref,n}$ to allow for demodulation of all channels simultaneously. In this way, individual lock-in signals and subsequent error signals are extracted for each frequency channel concurrently.

We built a dual-channel, frequency-locking NV magnetometer using a field-programmable gate array (FPGA) and a high-speed digital-to-analog-converter to digitally synthesize two carrier signals with frequencies that can be independently tuned and modulated. The generated signal is amplified and sent to a loop antenna to produce a MW field at the $2\text{ mm} \times 2\text{ mm}$ diamond sample, which contains a large ensemble of NV centers ($\sim 1 \times 10^{12}$). The diamond sample is optically excited with a 532-nm laser in a light-trapping diamond waveguide geometry for increased optical excitation efficiency.²³ Note, however, that the frequency-locking technique is applicable independent of measurement configuration and can be employed in a variety of different sample and measurement geometries. The NV fluorescence is collected with a balanced photodetector, where a pick-off from the laser is directed into the balancing port to remove common-mode laser noise. The lock-in amplifiers for demodulating the balanced photodetector signal and feedback compensators for locking to the NV resonances are also programmed into the FPGA, which continuously outputs the two locked frequencies to a computer.

Permanent magnets arranged in a Halbach array configuration produce a magnetic bias field $B_0 \approx 7.8\text{ mT}$, with $<0.1\%$ uniformity across the diamond. The orientation of the bias field with respect to the diamond axes serves to spectrally separate the resonances of the four NV classes. The dual-channel frequency-locking NV magnetometer then simultaneously locks to both the $m_s = 0 \rightarrow \pm 1$ transitions of a single NV orientation in order to decouple the effects of temperature and magnetic field to first order, and thus extract the magnetic field projection along the NV symmetry axis. To avoid depopulation and first order coherent driving effects, which affect the line shape,²⁶ different nuclear spin states are addressed for the upper and lower transitions.

Figure 2(a) demonstrates the frequency-locking NV magnetometer's robustness against changes in phenomenological variables, such as optical pump and MW drive power, which affect the contrast and linewidth of the ODMR spectra. We frequency lock to the $m_s = 0 \rightarrow \pm 1$ transitions of the NV orientation class that is most aligned to the applied magnetic field, using modulation frequencies $f_{\text{ref},1} = 1.8240\text{ kHz}$ and $f_{\text{ref},2} = 2.2813\text{ kHz}$ and modulation depths $f_{\text{dev},1,2} = 320\text{ kHz}$. By varying the optical pump power, e.g., the contrast of the ODMR resonance (upper inset) varies by more than an order of magnitude, which corresponds to varying slope in the lock-in signal (lower inset). In previous open-loop measurement techniques,^{6,22–24} this change in scale factor would result in a corresponding systematic error in magnetic field. Using the frequency-locking technique, while large variations in the optical pump power result in varying transient responses to a step input, the measured steady-state magnetic field remains consistent. The range of laser powers shown in Fig. 2(a) illustrates the robust nature of the frequency-locking method although practical MW and laser intensity fluctuations are smaller. In open-loop implementations, for example, a $\sim 5\%$ drift in laser intensity introduces an additional $\sim 5\%$ systematic error in the measured magnetic field, thus degrading the accuracy of an open-loop compared to a closed-loop NV magnetometer.

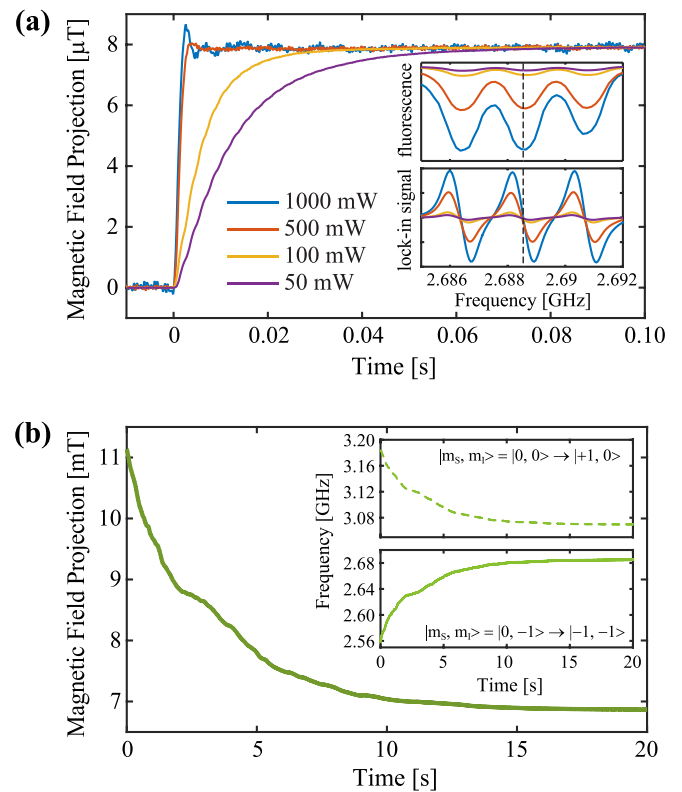


FIG. 2. (a) Magnetic field step response of Zeeman splitting showing that the same steady-state magnetic field is measured, independent of large differences in laser power. Upper inset: ODMR spectra of a single NV resonance. Lower inset: ODMR spectra at the output of the lock-in amplifier. The dashed vertical lines indicate the locked hyperfine transition. (b) The projection along an NV axis of the magnetic field produced by a free-moving permanent magnet varies by $>4\text{ mT}$ during a continuous acquisition. Simultaneous measurements of the upper and lower resonance frequency of a single NV orientation class are shown in the insets.

We employ a free-moving rare-earth permanent magnet to vary the magnetic field experienced by the frequency-locking NV magnetometer [Fig. 2(b)], demonstrating a dynamic range $\sim 4\text{ mT}$ in addition to the $\sim 7\text{ mT}$ bias field. A combination of the limited spatial access in the experimental apparatus and the need for a sufficiently uniform magnetic field across the diamond in order to avoid excessive broadening of the NV resonances constrained the permanent magnet in both size and proximity to the diamond, thus limiting the maximum measured field to $\sim 11\text{ mT}$. In contrast, in an open-loop lock-in based implementation, the dynamic range is limited to the linear region of the ODMR derivative signal, $\sim 2h\sigma/(10 g_e\mu_B)$, where σ is half of the linewidth of the NV resonance. For a typical $\sigma \approx 0.5\text{ MHz}$, the dynamic range is $\sim 4\text{ }\mu\text{T}$, three orders of magnitude less than the range demonstrated here. It is important to note that this increased dynamic range is not obtained at the expense of sensitivity, which we measure to be $\sim 1\text{ nT}/\sqrt{\text{Hz}}$ and is limited in our apparatus by experimental parameters (e.g., diamond material properties) that can be straightforwardly improved. While a dynamic range $\sim 4\text{ mT}$ was demonstrated here, in general, the dynamic range of the frequency-locking NV magnetometer is limited by the ambiguity when resonances of different NV orientation classes cross each other, which can be overcome by simultaneously detecting along all four possible diamond tetrahedral directions and performing

real-time analysis to take advantage of the redundancy of the overdetermined system. Ultimately, the dynamic range is limited by fluorescence suppression near the ground- and excited-state level anti-crossings at ~ 50 mT and ~ 100 mT.²⁷

Figure 3 illustrates the capability of the dual-channel frequency-locking NV magnetometer to measure vector magnetic fields. As before, a Halbach array of permanent magnets applies a uniform magnetic field over the NV ensemble within the diamond sample, causing Zeeman splitting in the $m_s = 0 \rightarrow \pm 1$ transitions of the four NV orientation classes and producing eight distinct NV resonances, each with three hyperfine transitions [Fig. 3(a)]. We simultaneously lock to the $|m_s, m_I\rangle = |0, -1\rangle \rightarrow |-1, -1\rangle$ and $|0, 0\rangle \rightarrow |+1, 0\rangle$ hyperfine transitions of a single NV orientation class (corresponding to the thin color-coordinated solid and dashed lines, respectively) and sequentially iterate through each NV orientation, with a 0.1-s dwell time per resonance pair. A set of three-axis Helmholtz coils apply additional $10 \mu\text{T}$ magnetic fields along three orthogonal directions. Figure 3(b) shows the resulting NV resonance frequency shifts detected using this method of locking to four pairs of NV transitions in rapid sequence. Using Eq. (1) and the known, rigid tetrahedral geometry of diamond crystal, we reconstruct the magnetic field vector by performing non-linear optimization of the overdetermined system, which results from measuring the magnetic field along four directions rather than three. The reconstructed magnetic field vector is presented in Fig. 3(c) and is in excellent agreement with the expected magnetic field produced by the calibrated

three-axis coils. Note that while we demonstrated full vector reconstruction by rapidly interleaving detection along each of the four possible NV orientation classes, simultaneous magnetic vector measurements can also be performed by extending the frequency-locking NV magnetometer's capability from two frequency channels to at least four,²⁴ thus increasing the speed at which the magnetic field vector can be reconstructed from being limited by the dwell time per resonance pair to the actual measurement speed.

The nitrogen-vacancy center in diamond possesses a wide range of properties that make it exceptionally suitable as a magnetometer: magnetic field measurements tied only to fundamental constants affording long-term stability,³ long room-temperature coherence times allowing for high sensitivity under ambient conditions,²⁸ a well-characterized temperature dependence enabling operation over an extreme thermal range,²⁰ high dynamic range, inherent vector capability tied to the stable diamond lattice,⁷⁻⁹ and a flexible solid-state geometry that supports a wide range of measurement modalities.^{5,6,23,29-31} In this work, we have addressed several key technical issues in order to realize many of these inherent capabilities in a single implemented device. We have demonstrated a multi-channel, simultaneous frequency-locking technique for scale-factor-free magnetic field measurements that are robust against temperature fluctuations, achieve high dynamic range, and are applicable to an NV ensemble for full reconstruction of the magnetic field vector. Such a demonstration marks a vital advance in transitioning the NV magnetometer from a laboratory system to a functional device for detecting fields in a practical environment.¹⁰⁻¹⁵

See [supplementary material](#) for a detailed derivation of the feedback loop dynamics and a measured noise density plot showing the magnetic sensitivity of the implemented device.

The authors thank J. Barry, C. McNally, and M. Walsh for helpful discussion. The Lincoln Laboratory portion of this work is sponsored by the Assistant Secretary of Defense for Research & Engineering under Air Force Contract No. FA8721-05-C-0002 and the Office of Naval Research Section 321MS. Opinions, interpretations, conclusions, and recommendations are those of the authors and are not necessarily endorsed by the United States Government. H.C. was supported by the NASA Office of the Chief Technologist's Space Technology Research Fellowship and the MIT LL Integrated Quantum Initiative. C.T. was supported in part by the AFOSR PECASE, supervised by Dr. Gernot Pomrenke, and the AFOSR MURI for Optimal Measurements for Scalable Quantum Technologies (FA9550-14-1-0052). D.E. acknowledges partial support from the Army Research Office Multidisciplinary University Research Initiative biological transduction program, Grant No. W911NF-17-1-0238.

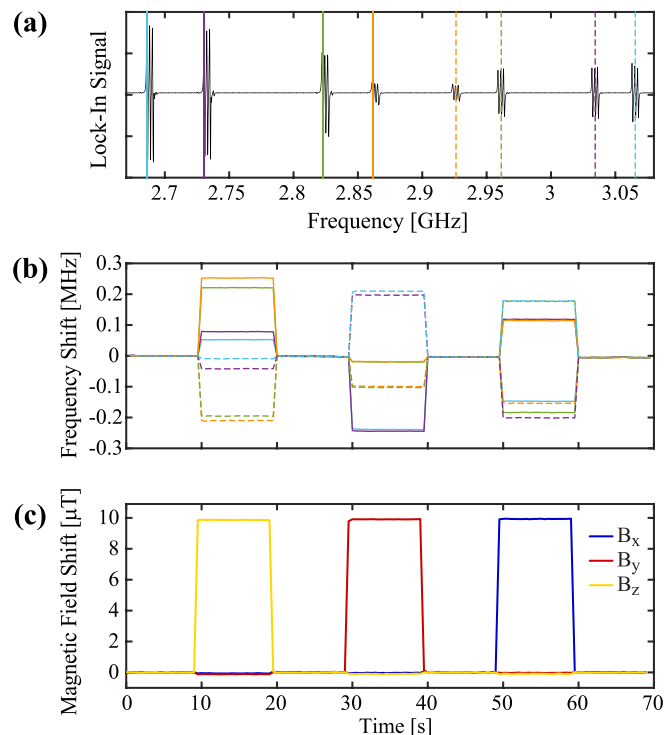


FIG. 3. (a) Lock-in ODMR spectrum showing all eight NV resonances. The colored vertical lines indicate the hyperfine transitions chosen for frequency-locking, with each different color corresponding to a single NV orientation class. Solid and dashed lines of the same color were locked simultaneously. (b) Frequency shifts of all eight NV resonances as a $10 \mu\text{T}$ field was applied sequentially in three orthogonal directions. (c) Magnetic field components reconstructed from the frequency shift data shown in (b).

¹I. K. Kominis, T. W. Kornack, J. C. Allred, and M. V. Romalis, *Nature* **422**, 596 (2003).

²D. Budker and D. Kimball, *Optical Magnetometry*, Optical Magnetometry (Cambridge University Press, 2013).

³J. M. Taylor, P. Cappellaro, L. Childress, L. Jiang, D. Budker, P. R. Hemmer, A. Yacoby, R. Walsworth, and M. D. Lukin, *Nat. Phys.* **4**, 810 (2008).

- ⁴V. M. Acosta, E. Bauch, M. P. Ledbetter, C. Santori, K.-M. C. Fu, P. E. Barclay, R. G. Beausoleil, H. Linget, J. F. Roch, F. Treussart *et al.*, *Phys. Rev. B* **80**, 115202 (2009).
- ⁵V. M. Acosta, E. Bauch, A. Jarmola, L. J. Zipp, M. P. Ledbetter, and D. Budker, *Appl. Phys. Lett.* **97**, 174104 (2010).
- ⁶J. F. Barry, M. J. Turner, J. M. Schloss, D. R. Glenn, Y. Song, M. D. Lukin, H. Park, and R. L. Walsworth, *Proc. Natl. Acad. Sci. U.S.A.* **113**, 14133 (2016).
- ⁷S. Steinert, F. Dolde, P. Neumann, A. Aird, B. Naydenov, G. Balasubramanian, F. Jelezko, and J. Wrachtrup, *Rev. Sci. Instrum.* **81**, 043705 (2010).
- ⁸B. J. Maertz, A. P. Wijnheijmer, G. D. Fuchs, M. E. Nowakowski, and D. D. Awschalom, *Appl. Phys. Lett.* **96**, 092504 (2010).
- ⁹L. M. Pham, D. L. Sage, P. L. Stanwix, T. K. Yeung, D. Glenn, A. Trifonov, P. Cappellaro, P. R. Hemmer, M. D. Lukin, H. Park *et al.*, *New J. Phys.* **13**, 045021 (2011).
- ¹⁰J. A. Shockley and J. F. Raquet, *Navigation* **61**, 237 (2014).
- ¹¹A. Canciani and J. Raquet, *IEEE Trans. Aerosp. Electron. Syst.* **53**, 67 (2017).
- ¹²R. S. Foote, *Relationship of Near-Surface Magnetic Anomalies to Oil and Gas-Producing Areas* (AAPG Special Volumes, 1996), Chap. 9, pp. 111–126.
- ¹³K. L. Kvamme, *Remote Sensing in Archaeology: An Explicitly North American Perspective* (University of Alabama Press, 2006), pp. 205–233.
- ¹⁴M. Espy, M. Flynn, J. Gomez, C. Hanson, R. Kraus, P. Magnelind, K. Maskaly, A. Matlashov, S. Newman, T. Owens *et al.*, *Supercond. Sci. Technol.* **23**, 034023 (2010).
- ¹⁵D. Sudac, D. Matika, and V. Valkovic, in *Proceedings of the 20th International Conference on the Application of Accelerators in Research and Industry* (AIP Publishing, 2009), Vol. 1099, pp. 574–577.
- ¹⁶R. S. Schoenfeld and W. Harnleit, *Phys. Rev. Lett.* **106**, 030802 (2011).
- ¹⁷M. S. Grinolds, M. Warner, D. Greve, K. Y. Dovzhenko, L. Thiel, R. L. Walsworth, S. Hong, P. Maletinsky, and A. Yacoby, *Nat. Nanotechnol.* **9**, 279 (2014).
- ¹⁸M. W. Doherty, N. B. Manson, P. Delaney, F. Jelezko, J. Wrachtrup, and L. C. Hollenberg, *Phys. Rep.* **528**, 1 (2013).
- ¹⁹L. Rondin, J.-P. Tetienne, T. Hingant, J.-F. Roch, P. Maletinsky, and V. Jacques, *Rep. Prog. Phys.* **77**, 056503 (2014).
- ²⁰V. M. Acosta, E. Bauch, M. P. Ledbetter, A. Waxman, L. S. Bouchard, and D. Budker, *Phys. Rev. Lett.* **104**, 070801 (2010).
- ²¹V. Stepanov, F. H. Cho, C. Abeywardana, and S. Takahashi, *Appl. Phys. Lett.* **106**, 063111 (2015).
- ²²C. S. Shin, C. E. Avalos, M. C. Butler, D. R. Trease, S. J. Seltzer, J. Peter Mustonen, D. J. Kennedy, V. M. Acosta, D. Budker, A. Pines *et al.*, *J. Appl. Phys.* **112**, 124519 (2012).
- ²³H. Clevenson, M. E. Trusheim, C. Teale, T. Schröder, D. Braje, and D. Englund, *Nat. Phys.* **11**, 393 (2015).
- ²⁴J. M. Schloss, J. F. Barry, M. J. Turner, and R. L. Walsworth, preprint [arXiv:1803.03718](https://arxiv.org/abs/1803.03718) (2018).
- ²⁵K. Jensen, V. M. Acosta, A. Jarmola, and D. Budker, *Phys. Rev. B* **87**, 014115 (2013).
- ²⁶P. Kehayias, M. Mrózek, V. M. Acosta, A. Jarmola, D. S. Rudnicki, R. Folman, W. Gawlik, and D. Budker, *Phys. Rev. B* **89**, 245202 (2014).
- ²⁷R. J. Epstein, F. M. Mendoza, Y. K. Kato, and D. D. Awschalom, *Nat. Phys.* **1**, 94 (2005).
- ²⁸G. Balasubramanian, P. Neumann, D. Twitchen, M. Markham, R. Kolesov, N. Mizuochi, J. Isoya, J. Achard, J. Beck, J. Tissler *et al.*, *Nat. Mater.* **8**, 383 (2009).
- ²⁹G. Balasubramanian, I. Y. Chan, R. Kolesov, M. Al-Hmoud, J. Tisler, C. Shin, C. Kim, A. Wojcik, P. R. Hemmer, A. Krueger *et al.*, *Nature* **455**, 648 (2008).
- ³⁰P. Maletinsky, S. Hong, M. S. Grinolds, B. Hausmann, M. D. Lukin, R. L. Walsworth, M. Loncar, and A. Yacoby, *Nat. Nanotechnol.* **7**, 320 (2012).
- ³¹J.-C. Jaskula, E. Bauch, S. Arroyo-Camejo, M. D. Lukin, S. W. Hell, A. S. Trifonov, and R. L. Walsworth, *Opt. Express* **25**, 11048 (2017).